Dynamics of Inter-Molecular Interactions Between Single $A\beta_{42}$ Oligomeric and Aggregate Species by High-Speed Atomic Force Microscopy

Lei Feng [1], Hiroki Watanabe [3], Paul Molino [1], Gordon G. Wallace [1], Son L. Phung [2], Takayuki Uchihashi [3] and Michael J. Higgins [1]

1 - ARC Centre of Excellence for Electromaterials Science, *Intelligent Polymer Research Institute, AIIM Facility, Innovation Campus, University of Wollongong, Wollongong, NSW 2522, Australia*
2 - School of Electrical, *Computer and Telecommunications Engineering, Faculty of Engineering and Information Sciences, University of Wollongong, Northfields Avenue, Wollongong, NSW 2522, Australia*
3 - Department of Physics, *Nagoya University, Higashiyama Campus, Furo-cho, Chikusa-ku, Nagoya 464-8602, Japan*

Correspondence to Michael J. Higgins: *ARC Centre of Excellence for Electromaterials Science, Intelligent Polymer Research Institute/AIIM Faculty, Innovation Campus, Squires Way, University of Wollongong, NSW 2522, Australia.* *mhiggins@uow.edu.au*
https://doi.org/10.1016/j.jmb.2019.04.044
Edited by Ronald Wetzel

Abstract

Within the amyloid hypothesis in Alzheimer's disease, current focus has shifted to earlier stages of amyloid beta (Aβ) peptide assembly, involving soluble oligomers and smaller aggregates, which are more toxic to cells compared to their morphological distinct fibril forms. Critical to the Aβ field is unlocking the molecular-level kinetic pathways of oligomerization, leading to the culprit subset or specific species of Aβ oligomer populations responsible for the disease etiology. Here, we apply high-speed atomic force microscopy to enable direct visualization of dynamic interactions between single $A\beta_{42}$ oligomers and aggregate forms, with combined nanometre structural and millisecond temporal resolution in liquid. Analysis of dimensions revealed up to three main $A\beta_{42}$ species distributions, in addition to the appearance of monomers that showed fast surface diffusion compared to the larger $A\beta_{42}$ species. Significantly, we devised a new single-molecule analysis based on image contrast in high-speed atomic force microscopy movies to quantify rate determining kinetic constants for interactions between the different $A\beta_{42}$ species. The findings revealed that smaller $A\beta_{42}$ species show an exponential decay of lifetime distribution, indicating that all molecules undergo the same process with a single well-defined energy barrier. In contrast, larger aggregates show randomized lifetimes, indicating a distribution of interactions energies/barriers that must be overcome in order to dissociate. We interpret the latter as being due to "permissive" binding, arising from different conformation states of the aggregates, along with a variety of accessible interacting groups. Inevitably, this may lead to the formation of different complexes or alloforms, which is known to contribute to difficulties in identifying Aβ oligomer toxicity and has implications for mechanisms underlying neuronal death accompanying Alzheimer's disease.

Introduction

Recent theory for pathogenies in Alzheimer's disease (AD) implicate the accumulation of soluble amyloid beta (Aβ) oligomers [1,2], generally consisting of low-molecular-weight monomeric, dimeric, tetrameric Aβ peptides [3], or higher-molecular-weight (~20 to 40 monomers) oligomers [4]. Due to their small size, high diffusion rate and permissivity to biological interactions, they are more highly toxic, particularly with high affinity for cellular ligands [5] such as neurosynapses. They are defined as basic proteins transformed into toxic forms that are structurally very distinct from their insoluble amyloid fibril successors found in plaques synonymous with AD [6,7]. Their increasing discovery in patients [8], along with a growing number of *in vitro* and animal studies demonstrating their toxicity [9,10], has seen a shift from earlier amyloid "cascade" hypotheses [11,12], based on plaque and fibril neurodegeneration, toward

understanding the protagonists of Aβ oligomer toxicity [7], including effects of size, morphology, homeostasis and biodistribution, leading to emergence of Aβ immunotherapies in clinical trials [13]. A fundamental challenge is identifying which subset or specific species of Aβ oligomers, among the apparent structural diversity and polymorphism with transient states, are responsible for AD. Equally as important to more broadly elucidate potential targets for AD therapies will be understanding the molecular interaction kinetics that ultimately define the oligomerization pathway(s) leading to the toxic populations.

Thioflavin T-based fluorescence kinetic studies on Aβ revealing classical sigmoid growth kinetics [14–16], including initial lag, followed by nucleation and fibril formation phases, enable quick interrogation of amyloid or fibrillation blockers, for example, antibodies, or the effects of amyloidogenic biological conditions such metal ion concentration [17,18] and pH [18,19]. The lag phase and slope of the nucleation phase partially indicates the rate at which oligomerization proceed; however, the kinetic contribution from specific, individual oligomer species is not discerned. From a structural perspective, x-ray crystallography, electron microscopy and atomic force microscopy (AFM) show that the oligomer species range from 2 to 50 nm in size [18,20], displaying diverse structures and assemblies. Emerging techniques such as ion mobility coupled with mass spectroscopy enable measurement of Aβ oligomer population distributions, revealing potential assembly pathways and specifically dodecamers as terminal species that are yet to rearrange into a β-sheet structures and thus may represent toxic forms in AD [20–22]. Single-molecule fluorescence measurements can probe oligomers present during the lag phase, showing they constitute a highly heterogeneous ensemble of species (~40 molecules) indicative of having undergone a stochastic polymer-like assembly process [23]. Up until now, only single-molecule force spectroscopy (SMFS) based on AFM is used to experimentally determine single molecule kinetics parameters (e.g., dissociation constants) of intra-molecular Aβ interactions [24]. Peptide functionalization of the AFM probe is currently only configured for the interaction between two monomers [25,26], effectively limiting measurements to dimerization kinetics. Exploring kinetics of very early stages of oligomerization, with seemingly fast transition states, are investigated by theoretical and computational simulations [27–29] in the absence of molecular-level experimental data.

To date, a significant mismatch exists between high-resolution structural imaging with poor temporal resolution *versus* inherently fast dynamic spectroscopy without the ability to directly visualize molecular structure. This is where the use of high-speed AFM (HS-AFM) provides a unique opportunity to study the molecular structural determinants of kinetics by decreasing structural imaging times of single molecules from minutes to milliseconds, that is, ~15–20 images per second [30–32]. Related to amyloid peptides, HS-AFM studies report on the structural flexibility of α-synuclein monomers and dimers associated with Parkinson's disease [33], dynamic formation of Aβ protofibrils [34], and structural dynamics of Aβ oligomers, including specified trimers, pentamers and heptamers [35]. Here, we develop a new analysis based on HS-AFM movies to produce lifetime traces, enabling the first extraction of kinetics assigned to inter-molecular interactions between different types of single-molecule Aβ$_{42}$ oligomers and aggregate forms. In doing so, we discover interesting kinetic phenomenon once the Aβ$_{42}$ species reach dimensions associated with larger aggregate species.

Results/Discussion

Structural dimensions of different Aβ$_{42}$ species

HS-AFM with scan sizes of 500 nm taken at imaging rates of 2 frames/s were used to characterize the structure and dimensions of the Aβ$_{42}$ peptide. A representative snapshot of a single frame at time t = 10 s revealed adsorbed peptides with a surface density of ~30–40 molecules/μm^2, primarily comprising small, globular-like structures of different sizes (Fig. 1a). Corresponding movies with duration of 500 s show the differently sized peptide species with varying surface diffusion speeds (Supplementary Movie S1). For statistical analysis of structural dimensions, MATLAB programs were developed to firstly separate the imported AVI movies into individual frames, then segment the objects in each frame via automatic thresholding, and lastly obtain the object parameters such as area (nm^2), width (nm), length (nm) and height (average pixel intensity; see the Methods section). Histogram analysis of the area showed three distinct peak distributions at 177 ± 60, 385 ± 94 and 670 ± 80 nm^2 (Fig. 1b), indicating the existence of at least three different forms of Aβ$_{42}$ peptide(s). From the width and length histograms (Fig. 1d and e), the main peak distributions occurred at 15.4 ± 3.2 and 19.6 ± 5.1 nm, respectively, indicating the size of the most abundant Aβ$_{42}$ peptide species. In addition, a second peak distribution occurred at higher values of 37.8 ± 2.1 nm, particularly for the width (Fig. 1d), and a similar distribution of values (36.9 ± 7.6 nm) is observed in skewed (non-normal; right tail) histogram of length (Fig. 1e). Two other main observations included a much smaller peak distribution between 6 and 12 nm (Fig. 1e, arrow) specifically for length and sampling of higher values of up to ~100 nm but with no clear distribution (Supplementary Fig. 1). For the height, two peak

distributions are observed at 2.85 ± 0.7 nm and another at 9.2 ± 2.5 nm (Fig. 1c).

The existence of these different Aβ$_{42}$ peptide species based on their size distributions indicates that the preparation of samples from lyophilized solid peptides dissolved in 1,1,1,3,3,3-hexafluoro-2-propanol (HFIP) does not result in pure monomers but instead leads to associated oligomers and larger aggregates [36,37]. This is somewhat contrary to the use of HFIP that constitutes a method typically used to minimize peptide aggregation. Once the peptides are resuspended in phosphate-buffered saline, they are immediately deposited onto the mica substrate for HS-AFM imaging (approximately after 20–30 min) and subsequently rinsed to remove excess free peptide. As mentioned the different Aβ$_{42}$ species do not form on the mica during imaging (they are pre-formed species in the sample solution) and the sample preparation also does not allow sufficient time for the formation of amyloid fibrils [38]. The latter enabled a focus on the interactions and dynamics of Aβ$_{42}$ monomers, oligomers and larger aggregates as opposed to the processes of fibril formation as done by several others in AFM studies [39,40].

Similar rounded structures of Aβ$_{42}$ peptide species with dimensions on the order of a few nanometres up to tens of nanometres are routinely observed in Aβ$_{40}$ and Aβ$_{42}$ samples in AFM studies [41,42]. Without the use of any solvent in the sample preparation, Prabhu *et al.* [43] similarly reveal a height range of 1.5–2.5 nm for Aβ$_{42}$ to explain the presence of either monomers or small oligomers. Using super sharp tips for AFM imaging, Mastrangelo *et al.* [4] refer to low-molecular-weight soluble Aβ$_{42}$ oligomers mostly with a height of ~1–2 nm and diameters ranging from 5 to 15 nm attributed to monomers or dimers (5–7 nm) and tetramers (~10–15 nm). In the same study based on the HFIP method, higher-molecular-weight (HMW) oligomers of 15–25 nm in diameter (reduced value after tip correction) with heights ranging from 3 to 6 nm indicated stacking of 2–3 monomers/dimers units. The HMW oligomers could also retain heights of 2 nm, suggesting the formation of planar structures [4]. More recently, Banerjee *et al.* [35] using HS-AFM show similar Aβ oligomer structures and distribution of sizes, including compact (5–7 nm), bilobed (20 nm) and larger aggregate structures, although they are differently assigned to specific trimers, pentamers and heptamers, respectively. A point of difference in this study is that a photochemical cross-linking method is used to enable isolation of Aβ according to their size

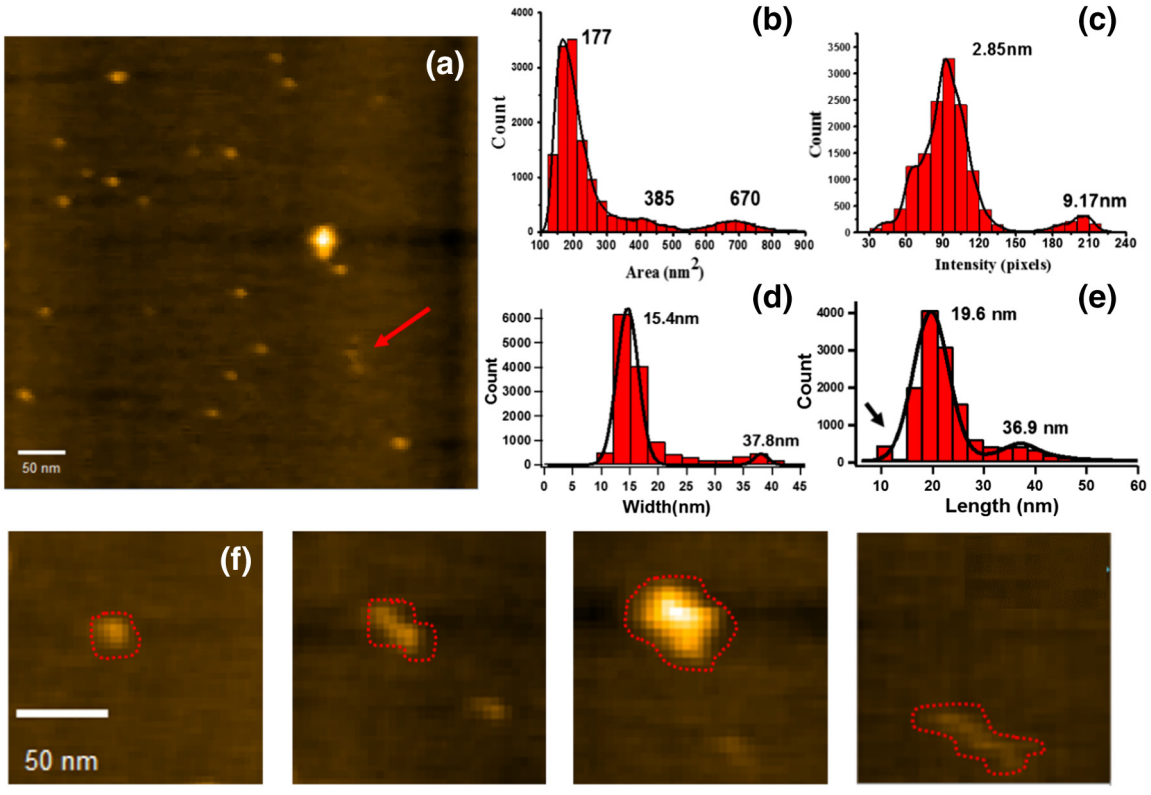

Fig. 1. Morphology and dimensions of Aβ$_{42}$. (a) Representative HS-AFM image frame at t = 10 s of Aβ species on mica surface in PBS (scan size: 500 nm, imaging rate: 2 frames/s). (b–e) Histograms of dimensions: area (b), height (c), width (d) and length (e). Peak values are from multi-peak fitting (Igor Pro, Wavemtrics). (f) Region of HS-AFM image frames showing representatives (from left to right) of Aβ$_{15–20\ nm}$, Aβ$_{36\ nm}$, Aβ$_{Agg}$ and disordered or unstructured Aβ species.

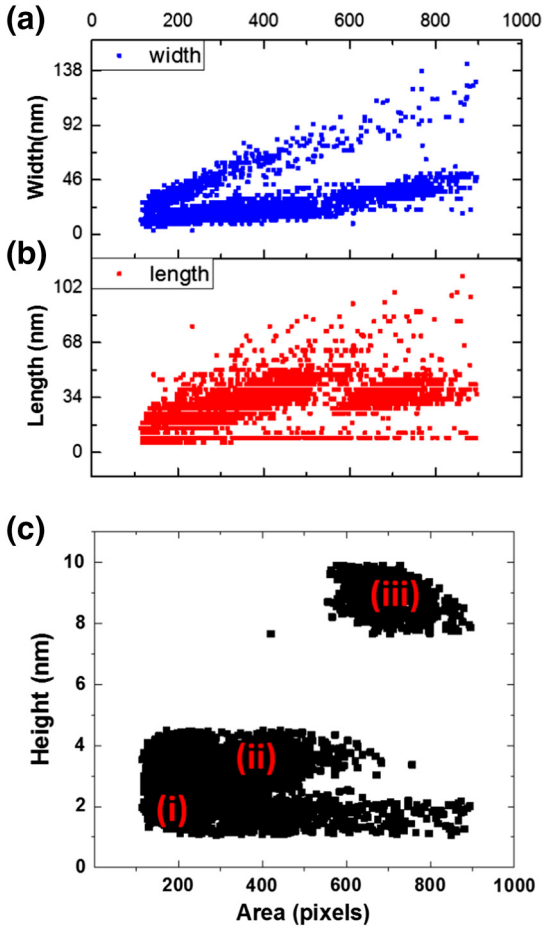

Fig. 2. Scatter plots of width (a), length (b), and height (c) *versus* area of Aβ species.

and purity, giving *a priori* knowledge of the sample distribution.

Theoretical and experimental measurements give a size of ~1–1.5 nm for single Aβ monomers [28,44,45]; thus, our HS-AFM observations show what appear to be mostly oligomers and larger aggregates. Previous AFM studies have shown that the lateral dimensions of Aβ, often up to tens of nanometers, exceed the most probable height of 2 nm and which is also the case in this study. Specifically, the lateral dimensions were shown to vary linearly with the height, suggesting that the latter is actually a true representation, that is, the Aβ is not perfectly spherical but more closely resemble oblate spheroids [46,47]. Despite this, tip broadening effects are expected to occur when the object's size is below the radius of tip curvature, and therefore, the lateral dimensions still represent an overestimation [42]. As mentioned above, similar sizes of Aβ$_{42}$ measured by AFM have previously been attributed to various forms, including pentamers, tetramers and HMW oligomers. Here, we refer to the most abundant distribution of Aβ species with an area of 180 nm^2, 15–20 nm (length–width) and height of 2.8 nm, as Aβ$_{15–20\ nm}$, since defining an exact number of monomer units is difficult. For example, in this compact structure (Fig. 1f, far left image), the individual monomers cannot be resolved due to insufficient AFM tip resolution. The next largest species correlating to an area of 385 nm^2 effectively relates to a doubling of size compared to Aβ$_{15–20\ nm}$. Despite the length–width histogram showing a second peak distribution at ~36–38 nm in Fig. 1d and e, its correlation to the distribution at 385 nm^2 could not be clearly determined. Therefore, additional histogram analysis was performed on length–width values categorized by only the 385-nm^2 distribution (Supplementary Fig. 2). Histograms show peak distributions of 34.4 ± 6.8 nm for length but only 16.5 ± 4.6 nm for width, indicating that this species had an elongated morphology as opposed to the rounded conformation of Aβ$_{15–20\ nm}$. The dimensions of this species, referred to as Aβ$_{36\ nm}$, is in accord with images showing a bilobed structure, consisting of two rounded, compact structures lying planar on the mica surface (Fig. 1f, middle left image). Interestingly, similar 20-nm bilobed structures were recently observed by Banerjee *et al.* [35] using HS-AFM and identified as pentamers produced using a photochemical cross-linking method. We interpret Aβ$_{36\ nm}$ as consisting of significantly more monomers, which also retain a height of 2.8 nm, indicating a planar structural configuration. The largest species giving a peak area distribution of 670 nm^2 and height distribution at 9.2 nm are clearly larger aggregates. Similarly to the above, histogram analysis performed on values categorized by only the 670-nm^2 area indicated that these species, referred to as Aβ$_{Agg}$ (Fig. 1f, middle right image), had length and width dimensions of 34.1 ± 10.7 and 35.7 ± 3.8 nm, respectively (Supplementary Fig. 2). Similar length–width dimensions were also confirmed by categorizing values by only the height distribution of 9.2 nm (Supplementary Fig. 2). Hence, it was evident that each of the species had overlapping distributions in their length–width dimensions. Furthermore, a small peak between 6 and 12 nm for length (Fig. 1e, arrow) combined with heights of ~1 nm is more closely indicative of dimensions equivalent to lower-molecular-weight oligomers such as dimers, trimers or tetramers, as described in previous AFM studies [48,49]. To date, a range of Aβ$_{42}$ oligomer structures, generally referred to as amyloid-beta derived diffusible ligands (ADDLs), globulomers and protofibrils, are described in several reviews [50–52]. Contrary to early theories on Aβ$_{42}$ existing in only stable monomeric or dimeric states, Teplow *et al.* and others [53,54] reveal a mixture of monomers, dimers, tetramers and HMW oligomers, specifically "paranuclei" (planar hexamers), stacked hexamers and dodecamers.

Additional less well, structurally defined Aβ$_{42}$ species, as opposed to the rounded conformations of Aβ$_{15–20\ nm}$, Aβ$_{36\ nm}$, Aβ$_{Agg}$, are observed transiently

appearing in the HS-AFM movies (Supplementary Movie S1), and a representative snapshot is given in Fig. 1f (far right image). However, due to their significantly lower heights of ~1 nm, they were not easily identified by automated threshold detection for analysis. In fact, they were most noticeable when observing movies as they appeared transiently, for example, flickering of the height contrast, in a scan area for <1–2 s, indicating their fast surface diffusion (Supplementary Movie S1). Supplementary Movie S2 indicates the appearance of these species by freezing the relevant frames. Separate AFM cross-sectional analysis show these Aβ$_{42}$ forms to be ~25.5 ± 4.4 nm in length and 1.1 ± 0.3 nm in height (Supplementary Fig. 3). We suggest that these forms are associated with significantly smaller, soluble Aβ$_{42}$ monomers that are known to be largely disordered or unstructured in solution [4], although the exact details of their transient conformational states or dynamics are unclear. Recent studies using FRET analysis show that both Aβ$_{40}$ and Aβ$_{42}$ comprise an ensemble of rapidly reconfiguring unfolded states, with no long-lived conformational states [55]. Molecular dynamic simulations support that the peptides have configurations consistent with random polymer chains, with the vast majority of conformations lacking significant secondary structure [45,56]. When considering tip broadening effects, the measured size of 25 nm correlates to an estimated contour length of an unfolded Aβ$_{42}$ monomer (i.e., 42 amino acids ~20 nm).

The relationship between the dimensional parameters (length, width, height, area) is shown in Fig. 2 to better understand the structural configurations of the different Aβ$_{42}$ species. Importantly, it is emphasized that Fig. 2 represents preformed Aβ$_{42}$ species arising from the sample preparation, that is, lyophilized peptide from HFIP followed by resuspension in PBS, as opposed to their formation after deposition on the mica surface. Two different linear trends for width (or length) *versus* area values are observed (Fig. 2a and b); the first trend (i) shows that as expected a change in width (or length) is proportional to the area. In contrast, the second trend (ii) shows a significantly smaller, or negligible increase in width (length) as a function of increasing area. This is due to the analysis method whereby the width and length are defined as increasing in value in the y-scan and x-scan directions, respectively. Thus, the effective width or length approaches zero if measured in the opposing scan direction. A height *versus* area plot reveals a region (i) where the height remains constant at just below ~2 nm with increasing area up to 800 nm^2 (Fig. 2c). This indicates that preformed aggregates can exist as planar structures with constant height and presumably form by the lateral addition of monomers. In contrast, regions (ii) and (ii) show an increase in height, firstly to ~3.5 nm and then ~9 nm, respectively (Fig. 2c). Specifically, the increase to 3.5 nm, while retaining the area of ~200 nm^2, suggests that this may be related to perpendicular reorientation of the larger Aβ$_{42}$ species, for example, Aβ$_{36\ nm}$, on the mica surface. At heights of 3.5 nm, further increases in the area to ~400 nm^2 indicate that the preformed aggregates can increase in size in both lateral and stacking directions. However, no further height increases are observed for areas of 200 and 400 nm^2. This interestingly leads to a "jump" in height and area of ~9 and ~600–800 nm^2, respectively, for the Aβ$_{Agg}$ (Fig. 2c). These changes in height as a function of area suggest that there is a formation of discrete, preformed Aβ$_{42}$ species, as opposed to randomly sized oligomers and aggregates, during the sample preparation of peptides.

Surface diffusion and interactions of different Aβ$_{42}$ species

MATLAB software was used to automatically track the motion of the different Aβ$_{42}$ species in movies (2 frames/s) for a duration of 20 s. In addition to MATLAB software analysis, representative filmstrips showing their diffusion are given in Fig. 3 and further corresponding movies in Supplementary Movies S3-S5. In each filmstrip, the solid colored circle delineates the current frame position of the individually tracked Aβ$_{42}$ species, while dashed circles denote the series of positions from the previous frames. Quantitative analysis of the mean square displacement (MSD) as a function of time for each Aβ species is plotted in Fig. 4a. Fitting to the slopes gives diffusion coefficients of 8.7 ± 0.44 nm^2 s^{-1} (Aβ$_{15–20\ nm}$), 1.1 ± 0.06 nm^2 s^{-1} (Aβ$_{36\ nm}$) and 0.4 ± 0.01 nm^2 s^{-1} (Aβ$_{Agg}$) (Fig. 4b), indicating that the Aβ$_{15–20\ nm}$ diffuses at a significantly greater speed than Aβ$_{36\ nm}$ and Aβ$_{Agg}$. Interestingly, "steps" are found in the slopes of Aβ$_{15–20\ nm}$ and this occurs to a lesser extent for Aβ$_{36\ nm}$ but is not observed for Aβ$_{Agg}$ (Fig. 4a). The steps are due to a significant increase in the MSD of the Aβ$_{15–20\ nm}$, within the period of a few frames. Following these steps, the Aβ$_{15–20\ nm}$ resumes its normal rate of diffusion. Reasons for the sudden bursts in diffusion speed are not fully clear, although they may relate to changes in surface absorption [57]. Further analysis of the fast diffusing monomers in Fig. 1f (far right image) and Supplementary Movie S2 was not undertaken because these peptides only existed in the scan area for a period of 1~2 frames, as mentioned above. In this case, the monomers are able to traverse an entire scan area of 500 nm within a few seconds, giving an estimated speed of >100 nm s^{-1} and diffusion coefficient of >2500 nm^2 s^{-1} (see Table 1)

Representative filmstrips show examples of commonly observed dynamic interactions between the different preformed Aβ species after having been deposited on the mica surface. i.e. Namely, where

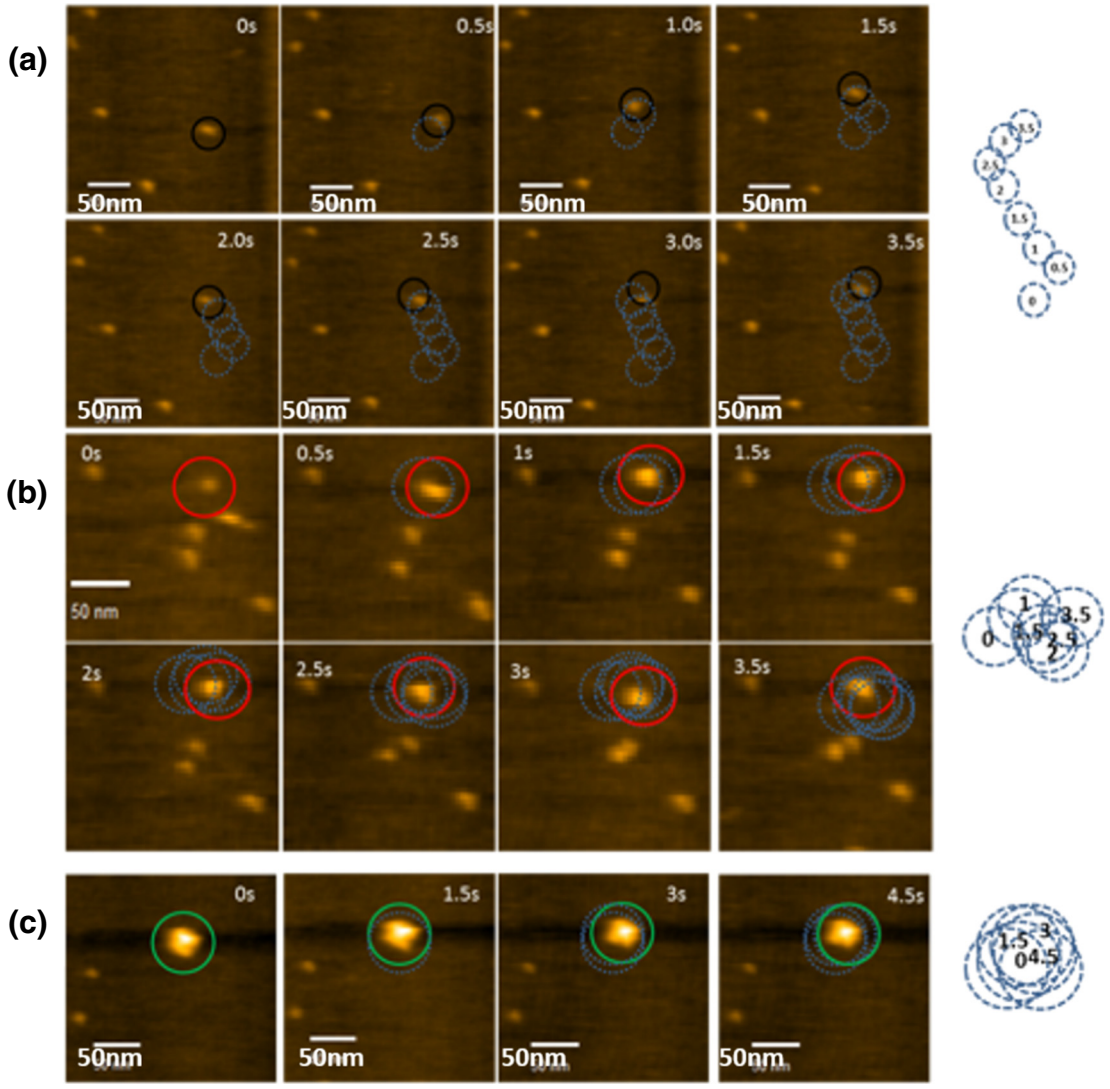

Fig. 3. Filmstrip from HS-AFM movies (imaging rate: 2 frames/s) showing the diffusion of individual Aβ$_{15–20\ nm}$ (a), Aβ$_{36\ nm}$ (b) and Aβ$_{Agg}$ (c) molecules. In each filmstrip, the solid colored circle delineates the current frame position of the individually tracked Aβ$_{42}$ species, while dashed circles denote the series of positions from the previous frames. Right-hand dashed circles show all positions from the corresponding filmstrip.

there was either 2D formation of elongated structures or addition of species in the z-direction giving increases in height (Fig. 5). For example, after 0.8 s, an Aβ$_{15–20\ nm}$ (2) moves closer to an Aβ$_{Agg}$ (3) until they undergo binding at 1.4 s and remain as a complex (2 + 3) for the remainder of the filmstrip (Fig. 5a). In this case, the complex (2 + 3) increases in width–length (and area). At 1.6 and 3.4 s, further interactions within the complex (2 + 3) show the Aβ$_{15–20\ nm}$ "rebinding" to the top of the Aβ$_{Agg}$, causing an increase in height (stacking in Fig. 5a) but no significant change in the area. Following this in Fig. 5b, Aβ$_{15–20\ nm}$ (1) and a new Aβ$_{15–20\ nm}$ (4) enter the scan area and both interact with complex (2 + 3) (4.0 s), resulting in elongation and formation a small, protofibril-like structure. To visualize the dynamics of the entire process, see Supplementary Movie S6. These collective interactions involve interactions occurring in the z-direction (2 ↔ 3) and x–y direction (1 ↔ complex (2 + 3) ↔ 4), demonstrating a combined growth process to form new Aβ species. In general, these types of interactions are dynamic and qualitatively could be either short-lived or long-lived; for example, the proto-fibril structures were only transient compared to newly formed, more stable oligomer and aggregate complexes.

Kinetic parameters of single-molecule Aβ42 binding

The ability to directly "watch" single-molecule interactions in action between the different Aβ$_{42}$ species provides a unique opportunity to quantify

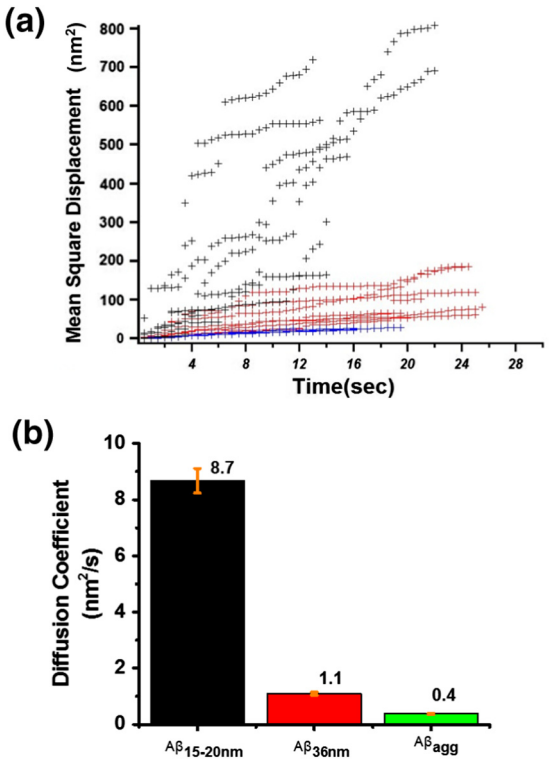

Fig. 4. (a) MSD *versus* time plot of individually tracked $A\beta_{15–20\ nm}$ (black), $A\beta_{36\ nm}$ (red) and $A\beta_{Agg}$ (blue) molecules. MSD = $<|\ r(t) - r(0)\ |^2>$,where $<\ >$ means the average, $r(t)$ is the position of each molecule in determined time t, $r(0)$ is the reference position of each molecule. (b) Average diffusion coefficient of 8.7 ± 0.44 nm^2 s^{-1} ($A\beta_{15–20\ nm}$), 1.1 ± 0.06 nm^2 s^{-1} ($A\beta_{36\ nm}$) and 0.4 ± 0.01 nm^2 s^{-1} ($A\beta_{Agg}$) obtained by fitting slopes in panel a. Errors are standard deviation, n = >10 molecules.

kinetics underlying the process of oligomerization. Here, we quantify the binding kinetics by measuring the amount of time two molecules spend in physical contact, which is defined by the formation of image contrast between the two molecules. Significantly, we extract kinetic parameters, including, mean lifetime $<t>$ and dissociation rate constant, k_{off} ($1/<t>$), for specific interactions between the $A\beta_{15–20\ nm} \leftrightarrow A\beta_{15–20\ nm}$, $A\beta_{15–20\ nm} \leftrightarrow A\beta_{36\ nm}$, and $A\beta_{15–20\ nm} \leftrightarrow A\beta_{Agg}$ (Fig. 6a–c). An important distinction for this type of HS-AFM-based analysis is involvement of the peptide–mica surface interaction and its role in diffusion-limited effects on the intrinsic association and dissociation rates of the Aβ species. For instance, the Aβ species can come in contact via diffusion, after which they undergo binding at a rate governed by their intrinsic association rate constant. Conversely, the Aβ species dissociate with an intrinsic rate constant, after which they move apart via diffusion. Therefore, the time spent in contact between two species may be influenced by diffusion, which as shown in Fig. 3 differs depending on the size of the Aβ species.

For this analysis, the binding is directly visualized as being "on" or "off" (Fig. 6a–c) to produce single-molecule lifetime traces (Fig. 6d–f) that are analogous to those commonly obtained using fluorescence techniques, for example, single-molecule FRET [57,58]. Supplementary Movies S7–S9 show corresponding movies of the different Aβ interactions represented in filmstrips in Fig. 6a–c. Lifetime distributions for the bound state show a single exponential decay law for the $A\beta_{15–20\ nm} \leftrightarrow A\beta_{15–20\ nm}$ and $A\beta_{15–20\ nm} \leftrightarrow A\beta_{36\ nm}$ (Fig. 6h–i), indicating a single-step binding process that yields one characteristic lifetime for these types of interactions. A mean lifetime $<t>$ = 0.55 ± 0.22 s, with dissociation rate constant k_{off} ($1/<t>$) = 2.17 ± 0.87 s^{-1}, for the $A\beta_{15–20\ nm} \leftrightarrow A\beta_{15–20\ nm}$ compared to the $A\beta_{15–20\ nm} \leftrightarrow A\beta_{36\ nm}$ with a mean lifetime = 0.72 ± 0.28 s (k_{off} = 1.64 ± 0.64 s^{-1}), indicating the latter to some extent forms more tightly bound complexes due to its slower dissociation rate. It could also be that the slower dissociation rate is partially governed by diffusion, whereby with the order of the magnitude slower diffusing $A\beta_{36\ nm}$ on the mica surface, even weaker interactions are sufficient to keep them in contact for measurable periods of time. In contrast, lifetime distributions for the $A\beta_{15–20\ nm} \leftrightarrow A\beta_{Agg}$ show a randomized histogram of shorter-lived through to longer-lived complexes (Fig. 6g), indicating a distribution of interactions energies or barriers that the $A\beta_{15–20\ nm} \leftrightarrow A\beta_{Agg}$ complex must overcome in order to dissociate. When considering the effects of diffusion, the $A\beta_{Agg}$ is also an order of magnitude slower compared to the $A\beta_{15–20\ nm}$ and effectively static on the mica surface, with the $A\beta_{15–20\ nm}$ acting as a faster diffusing ligand. Under these conditions, the $A\beta_{15–20\ nm}$ diffusion may influence the dissociation rate; however, it is not expected to significantly alter the energy landscape of the unbinding pathway(s). Thus, the randomized histogram is suggested to be intrinsic to the $A\beta_{15–20\ nm} \leftrightarrow A\beta_{Agg}$ interaction. This is different from an exponential decay of lifetimes, indicating that all molecules undergo the same process with a single well-defined energy barrier, as the case for the $A\beta_{15–20\ nm} \leftrightarrow A\beta_{15–20\ nm}$ and $A\beta_{15–20\ nm} \leftrightarrow A\beta_{36n}$ complexes in Fig. 6h–i.

Kinetic parameters for single-molecule Aβ peptide interactions have only previously been determined by another AFM-based technique, SMFS. For the SMFS, a monomeric peptide is attached to a substrate, for example, via a heterobifunctional cross-linker molecule such as *N*-hydroxysuccinimide-polyethylene glycol-maleimide [59], and the opposing monomer is bound to the AFM cantilever tip [60]. By bringing the peptide functionalized tip into contact with the substrate, the measurement of single-molecule unbinding forces as a function of the loading rate, referred to as dynamic force spectroscopy (DFS), enables kinetic

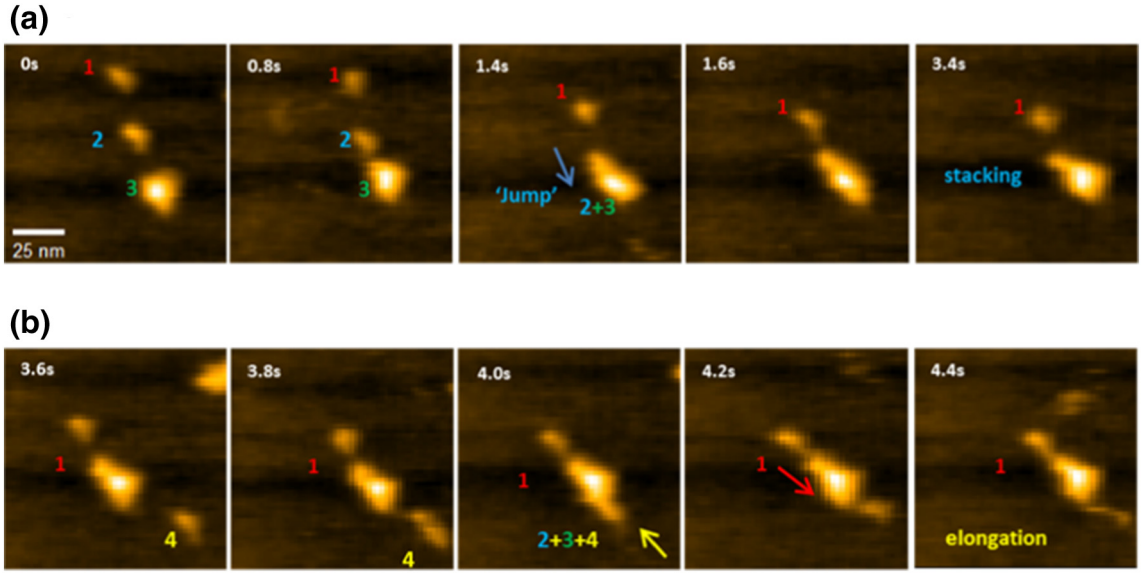

Fig. 5. Filmstrip from HS-AFM movies showing (a) sequence of interactions between Aβ$_{15–20\ nm}$ (1 and 2) and Aβ$_{Agg}$ (3) involving binding of Aβ$_{15–20\ nm}$ (2) on top of Aβ$_{Agg}$ (3) (stacking to form complex 2 + 3). (b) Continuation of sequence in panel a showing formation of elongated structure due to interactions of Aβ$_{15–20\ nm}$ (1 and 4) with complex (2 + 3). The scale bar represents 25 nm. Imaging rate: 5 frames/s.

and thermodynamic parameters to be extracted, yielding a useful comparison of k_{off} and bond lifetimes. Yu *et al.* [26] carried out DFS measurements to understand the amyloid-related misfolding and aggregation of α-synulein in Parkinson's disease. At pH 5, a single energy barrier to unbinding of single α-synuclein monomers, or dimer dissociation, gave k_{off} of ~3.74 ± 1.99 s^{-1} with lifetimes of 0.27 s. More weakly bound Aβ$_{40}$ monomer–monomer interactions give k_{off} of ~9.4 ± 1.50 s^{-1} with shorter lifetimes of 0.1 ± 0.01 s at pH 7 [61]. Lv *et al.* [24] compared both Aβ$_{40}$ and Aβ$_{42}$, giving k_{off} of 9.0 ± 2.4 s^{-1} (0.11 ± 0.03 s) and 5.7 ± 0.3 s^{-1} (0.18 ± 0.01 s), respectively, revealing stronger inter-peptide interactions for Aβ$_{42}$ than for Aβ$_{40}$ [62]. Specifically for Aβ$_{42}$ monomer–monomer unbinding, Hane *et al.* [63] tested multiple DFS models (Bell–Evans and Friddle–De Yoreo), giving k_{off} of ~7-12 s^{-1} with lifetimes of 0.14–0.09 s, while comparable k_{off} of ~12.5 ± 9.62 s^{-1} and lifetimes of 0.09 ± 0.7 s were obtained in a further study on the effect of copper ions

Table 1. Summary of properties of different Aβ species

Summary of Aβ properties	Aβ$_{15–20\ nm}$	Aβ$_{36\ nm}$	Aβ$_{Agg}$	Unstructured Aβ
			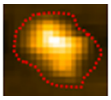	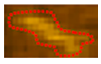
Width (nm)	15.4 ± 3.2	16.5 ± 4.6	35.7 ± 3.8	–
Length (nm)	19.0 ± 5.1	34.4 ± 6.8	34.1 ± 10.7	25.5 ± 4.4[a]
Height (nm)	2.8 ± 0.7	2.8 ± 0.7	9.2 ± 2.5	1.1 ± 0.3[a]
Area (nm^2)	177 ± 60.4	385 ± 93.8	670 ± 80.4	–
Diffusion coefficient ($nm^2\ s^{-1}$)	8.7 ± 0.44	1.1 ± 0.06	0.4 ± 0.01	>2500[a]
Lifetime (s)	0.55 ± 0.22[b]	0.72 ± 0.28[c]	[d]	–
k_{off} (s^{-1})	2.17 ± 0.87[b]	1.64 ± 0.64[c]	[d]	–

Width, length and height values of Aβ$_{15–20\ nm}$, Aβ$_{36\ nm}$, and Aβ$_{Agg}$ obtained from histograms in Fig. 1 and Supplementary Fig. 2. Extraction of values from HS-AFM videos using MATLAB algorithm of automated threshold detection. Peak values and error (fit width) are obtained from multi-peak fitting (Igor Pro, Wavemtrics).

[a] For the unstructured Aβ, length and height values obtained by cross-sectional analysis in HS-AFM software (Wavemetrics, Igor Pro). Diffusion coefficient estimated from diffusion speed of 100 nm/s; therefore, MSD > 100 nm^2. For diffusion coefficient, D = MSD/4t, then $D > 10^4/4 = 2500\ nm^2\ s^{-1}$. Errors are standard deviation.

[b] Lifetime and k_{off} for interactions between Aβ$_{15–20\ nm}$ ↔ Aβ$_{15–20\ nm}$.

[c] Lifetime and k_{off} for interactions between Aβ$_{36\ nm}$ ↔ Aβ$_{15–20\ nm}$. Errors from fitting exponential decay in Fig. 6h and i.

[d] Aβ$_{36\ nm}$ show randomized lifetime histograms; thus, no lifetime and k_{off} is obtained.

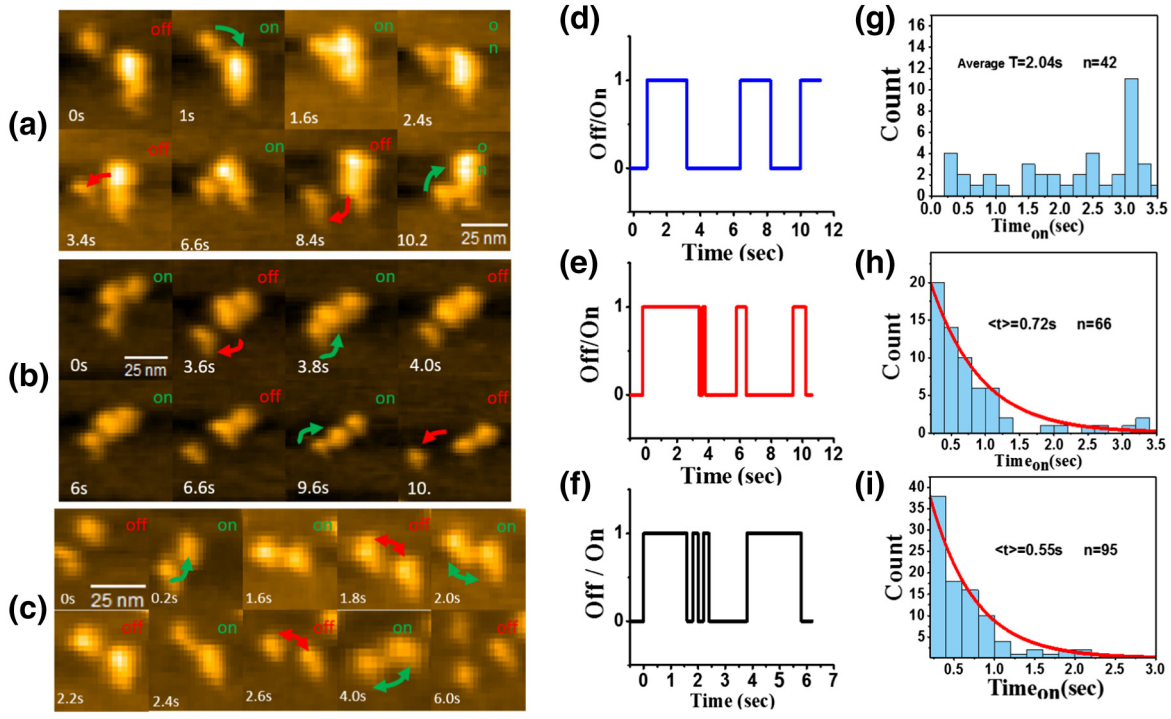

Fig. 6. Single-molecule kinetics data analysis based on HS-AFM. (a–c) HS-AFM filmstrips showing interactions between (a) Aβ$_{15–20\ nm}$–Aβ$_{Agg}$, (b) Aβ$_{15–20\ nm}$–Aβ$_{36\ nm}$ and (c) Aβ$_{15–20\ nm}$–Aβ$_{15–20\ nm}$. Molecules in contact are in the bound state (green 'on). Imaging rate: 5 frames/s. (d–e) Representative traces of single-molecule lifetimes for (d) Aβ$_{Agg}$, (e) Aβ$_{36\ nm}$ and (f) Aβ$_{15–20\ nm}$. (g–i) Lifetime distributions for the bound state of (g) Aβ$_{15–20\ nm}$–Aβ$_{Agg}$, (h) Aβ$_{15–20\ nm}$–Aβ$_{36\ nm}$ and (i) Aβ$_{15–20\ nm}$–Aβ$_{15–20\ nm}$. Distributions in panels h and i are fit to a single exponential decay.

[64]. From these SMFS studies, it is now understood that Aβ dimeric complexes have high stability, dissociating over a period of seconds, that is, ~5–12 s^{-1}, due to the monomers adopting antiparallel binding structures as shown in MD simulations [65]. This is very different from intramolecular interactions of monomers that occur on much shorter micro-to-nanoseconds timescales [66], suggesting that the dimerization process measured in SMFS may be an important protagonist in the early aggregation process. To date, the peptide functionalization in SMFS studies is only configured for the interaction between two monomers [25,26] such as in dimerization, although it is expected that clever functionalization strategies in the future will enable SMFS on a range of Aβ oligomer structures. Using our HS-AFM-based analysis theoretically allows for kinetic information on a multitude of combinatorial Aβ interactions, including those consisting of multiple monomer units.

Conclusions

HS-AFM analysis suggests that the formation of aggregates such as Aβ$_{Agg}$ is driven by kinetic heterogeneity, indicating a shift in the mechanism of oligomerization. We liken this to "opportunistic" or permissive binding, arising from different conformation states of the Aβ$_{Agg}$, along with a variety of accessible interacting groups. Inevitably, this will likely lead to the formation of different complexes or alloforms, which is known to contribute to the complexity and challenges in identifying Aβ oligomer toxicity. Equally for ensemble kinetic measurements, nucleation-limited aggregation of Aβ(1–40) peptide is shown to be controlled by a stochastic factor inherent in the nucleation process, leading to substantial macroscopic heterogeneity [67]. More recently, Nag *et al.* [68] refer to "metastable" Aβ$_{40}$ oligomers that are thermodynamically unstable but show a large kinetic barrier, which is mostly entropic in origin. The monomers are said to be entangled in the initial oligomeric state, with multiple intra- and intermolecular hydrophobic interactions aiding in their entanglement. At the single-molecule level, Orte *et al.* [69] recently report on stochastic behavior in early stages of oligomer fibril formation by the SH3 domain from bovine phosphatidylinositol-3-kinase (PI3–SH3). Using two-color single-molecule fluorescence, they show that, although the size distribution of detected SH3 oligomers remains virtually constant with increasing aggregation time, they constitute a highly heterogeneous ensemble of species, which is explained by a stochastic polymer-like assembly process [69]. Molecular dynamics simulations of the early steps of aggregation provide evidence that the associating and initially monomeric polypeptide chains can sample and

stabilize early aggregates of considerably different structures [70], with considerable conformational flexibility, thereby enabling the formation of very different conformational arrangements [71]. Such observations are a testament to oligomers possessing a high degree of polymorphism, as a result of stochastic fluctuations in polypeptide chain dynamics. Evidence is increasingly pointing to heterogeneity as a protagonist in aggregation. For example, variations in oligomer conformation and associated interactions, and not just specificity in oligomer size, may be responsible for biological toxicity, as demonstrated for HypF-N protein [72]. Our study contributes to this emerging narrative by quantifying the kinetic parameters of different Aβ species consisting of oligomers and aggregate forms, in particular confirming a distinct change in the energy (binding) landscape occurring at the onset of interactions with larger aggregate species.

In conclusion, single-molecule kinetic data can make significant contributions to "kinetic" distribution models that depict aggregation pathways, but which still lack the assignment of fully quantitative kinetic constants to their various pathways. Table 1 shows a summary of properties of the different Aβ$_{42}$ species, and their dimensions can now be correlated to the dynamic properties such as diffusion and interaction kinetics. In particular, HS-AFM movies emphasize the dynamic, transient states that exist within and between the different species. In assimilating to current models, the findings show that interactions between smaller Aβ species (Aβ$_{15–20\ nm}$ and Aβ$_{36\ nm}$) present a single exponential decay of lifetimes, while interactions with larger aggregates are driven by a type of kinetic heterogeneity. The latter enables the formation of long-lived, stable Aβ aggregates. It is necessary in future HS-AFM studies to investigate the influence of peptide-surface interactions and diffusion parameters on quantitative analysis of kinetic parameters, although such studies are also relevant to the effects of cell membrane surfaces and other intracellular substrates that may play a role in the formation of Aβ oligomers/aggregates. In addition, implementing well-defined Aβ peptides, for example, comprising recombinant peptides or those with structures known *a priori*, will assist in rationalizing AFM characterization of peptide dimensions and together with new insights on Aβ dynamics from HS-AFM, exciting advances in understanding Aβ$_{42}$ interactions can be explored.

Methods

Preparation of Aβ solutions and reagents

Amyloid-beta protein fragment 1–42 (Aβ$_{42}$ peptide) was purchased as a lyophilized solid, and more than 95% purity was guaranteed by HPLC from Sigma-Aldrich (High Performance Liquid Chromatography). ADDL's from Aβ$_{42}$ peptide were prepared according to previous methods of Refs. [4,73]. Firstly, 1-mg lyophilized solid peptides were dissolved in HFIP to prevent aggregation and then aliquoted into 50 small microcentrifuge tubes. After 30-min incubation at room temperature in a chemical fume hood, the HFIP was allowed to evaporate for 60 min and the re-lyophilized peptides stored at $^{-}$20 °C. Aqueous solutions were prepared by dissolving peptides into PBS (pH 7.4) at concentration of 20 μg/ml and then vortex mixing for 20 s prior to use.

Remodification of HS-AFM cantilever tips

High-resonance frequency (0.8–1.2 MHz) cantilevers with low spring constants (0.1–0.2 Nm^{-1}) specially designed for HS-AFM imaging were obtained from Olympus (BL-AC10DS). The silicon cantilevers consisted of a beak-like tip upon which we further deposited a carbon-based tip by electron-beam deposition. The carbon tip was sharpened by argon or oxygen plasma etching to produce a significantly smaller tip radius of ~3 nm compared to the original tip (25–100 nm) of the commercial cantilever, which enabled improved imaging stability and resolution [74,75]. After imaging, the carbon tip could be completely removed by plasma etching and the cantilever remodified for reuse.

HS-AFM imaging in liquid

To prepare samples for imaging, 2 μl of 20 μg/ml Aβ$_{42}$ peptide in PBS was pipetted onto a 1.5-mm-diameter freshly cleaved mica disc (Cat. No. 7101) and incubated for 2 min. Two microliters of fresh PBS was then added and pipetted in/out of the sample solution, and this was repeated several times to exchange the sample solution in order remove excess Aβ$_{42}$ peptides that had not adsorbed onto the mica surface. The sample was then placed into the liquid cell for HS-AFM imaging. HS-AFM imaging was performed using an ANDO-model (Research Institute of Biomolecule Metrology Co., Ltd., Japan) in tapping mode with high-frequency, small cantilevers (BL-AC10, Olympus) remodified with the carbon tip, as described above. During imaging, the free oscillation amplitude of the cantilever was set to ~2 nm and the set point amplitude was kept to ~90% of the free amplitude. An XY scanner with a range of 4 μm × 4 μm and z scanner (700 nm) with scan speeds of normally 2–4 frames/s for 500-nm scans was used. For higher-resolution scans of 200 nm, a scan speed of 5–10 frames/s was applied. During imaging, a relatively large gain force can be applied without affecting the interactions to improve the image quality owing to the short time of force action (~100 ns). Thus, in the experiment, different types of dynamic events

occurring in the biological environment can be visualized.

Data analysis of HS-AFM movies

A MATLAB computer program was developed to segment molecules in HS-AFM images. The program had four main stages: (1) background image estimation, (2) background subtraction and contrast enhancement, (3) image segmentation using the Otsu's algorithm, (4) connected component labeling and object measurement.

In stage 1, the background image was estimated by applying image erosion followed by image dilation. Let $I(x, y)$ be an input HS-AFM image, where x and y are the horizontal and vertical coordinate, respectively. To compute the eroded image I_e, the pixel at location (x, y) was set as the *minimum* of all pixels in a local neighborhood of image I:

$$I_e(x, y) = \mathbf{min} I(R(x, y))$$

In our experiments, the local neighborhood R was selected as a circular region of radius 15 centred at pixel location (x, y). Next, to compute the dilated image I_b, the pixel at location (x, y) was set as the *maximum* of all pixels in a local neighborhood of image I_e:

$$I_b(x, y) = \mathbf{min} I_e(R(x, y))$$

The dilated image $I_b(x, y)$ was considered as estimation of the image background.

In stage 2, the background image was subtracted from the input image: $I_d = I - I_b$. The difference image I_d contained mostly the foreground (i.e., the molecules). To improve the contrast of the foreground and consequently the segmentation accuracy, the difference image I_d was scaled linearly to the full intensity range [0, 255]. In stage 3, the enhanced difference image was segmented using the Otsu's algorithm. In this algorithm, a threshold is applied to separate the image into two classes: foreground and the image background. This threshold is selected to minimize the intra-class variance and maximize the inter-class variance and. In other words, this algorithm increases the similarity between pixels belonging to the same class while decreases the similarity between pixels belonging to different classes. In stage 4, connected component labeling was applied to each group of connected pixels into a single region (molecule). For each region, several properties were measured, including width, height, bounding-box coordinates, centroid, perimeter, area and eccentricity. In addition, the length and width of peptides were validated using the cross-section analysis in the Igor Pro software. Using the above properties, molecules were also tracked across multiple frames of a HS-AFM video sequence.

We also applied filters to some videos, especially for the height measurement, to better observe the individual molecules and their dynamic interactions. As a result, some darker regions may appear in these snapshot images and slightly affect the real height value of peptides that are adsorbed in these darker areas. We then performed analysis manually using line height profile in Igor Pro with the filter on *versus* off to calculate a correction factor for the height data.

Supplementary data to this article can be found online at https://doi.org/10.1016/j.jmb.2019.04.044.

Acknowledgments

The authors are grateful for the support of the Chinese Scholarship Council. Funding from the Australian Research Council Centre of Excellence Scheme (Project Number CE 140100012) is gratefully acknowledged. The authors would like to thank the Australian National Fabrication Facility–Materials node for equipment use.

Received 25 February 2019;
Received in revised form 12 April 2019;
Available online 07 May 2019

Keywords:
amyloid beta peptide;
Alzheimer's disease;
oligomerization;
single molecule kinetics;
high-speed atomic force microscopy

Abbreviations used:
AD, Alzheimer's disease; Aβ, amyloid beta; SMFS, single-molecule force spectroscopy; HS-AFM, high-speed atomic force microscopy; HFIP, 1,1,1,3,3,3-hexafluoro-2-propanol; HMW, higher molecular weight; MSD, mean square displacement; DFS, dynamic force spectroscopy.

References

[1] J.A. Hardy, G.A. Higgins, Alzheimer's disease: the amyloid cascade hypothesis, Science 256 (5054) (1992) 184.
[2] W.L. Klein, Aβ toxicity in Alzheimer's disease: globular oligomers (ADDLs) as new vaccine and drug targets, Neurochem. Int. 41 (5) (2002) 345–352.
[3] S.M. Catalano, E.C. Dodson, D.A. Henza, J.G. Joyce, G.A. Krafft, G.G. Kinney, The role of amyloid-beta derived diffusible ligands (ADDLs) in Alzheimer's disease, Curr. Top. Med. Chem. 6 (6) (2006) 597–608.
[4] I.A. Mastrangelo, M. Ahmed, T. Sato, W. Liu, C. Wang, H. Paul, S.O. Smith, High-resolution atomic force microscopy of soluble Aβ42 oligomers, J. Mol. Biol. 358 (1) (2006) 106–119.

[5] Y. Gong, Chang Lei, Kirsten L. Viola, Pascale N. Lacor, Mary P. Lambert, Caleb E. Finch, et al., Alzheimer's disease-affected brain: presence of oligomeric Aβ ligands (ADDLs) suggests a molecular basis for reversible memory loss, Proc. Natl. Acad. Sci. U. S. A. 100 (18) (2003) 10417–10422.
[6] I.W. Hamley, The amyloid beta peptide: a chemist's perspective. Role in Alzheimer's and fibrillization, Chem. Rev. 112 (10) (2012) 5147–5192.
[7] C.G. Glabe, R. Kayed, Common structure and toxic function of amyloid oligomers implies a common mechanism of pathogenesis, Neurology 66 (1 suppl 1) (2006) S74.
[8] H. Braak, E. Braak, J. Bohl, Staging of Alzheimer-related cortical destruction, Eur. Neurol. 33 (6) (1993) 403–408.
[9] Robin D. Johnson, Joseph A. Schauerte, Chang Chun-Chieh, Kathleen C. Wisser, John Christian Althaus, Cynthia J.L. Carruthers, et al., Single-molecule imaging reveals Aβ42:Aβ40 ratio-dependent oligomer growth on neuronal processes, Biophys. J. 104 (4) (2013) 894–903.
[10] S. Lesné, Ming Teng Koh, Linda Kotilinek, Rakez Kayed, Charles G. Glabe, Austin Yang, et al., A specific amyloid-β protein assembly in the brain impairs memory, Nature 440 (2006) 352.
[11] Holtzman, D.M., C.M. John, and A. Goate, Alzheimer's disease: the challenge of the second century. Science translational medicine, 2011. 3(77): p. 77sr1-77sr1.
[12] T.E. Golde, L.S. Schneider, E.H. Koo, Anti-Aβ therapeutics in Alzheimer's disease: the need for a paradigm shift, Neuron 69 (2) (2011) 203–213.
[13] F. Mangialasche, A. Solomon, B. Winblad, P. Mecocci, M. Kivipelto, Alzheimer's disease: clinical trials and drug development, The Lancet Neurology 9 (7) (2010) 702–716.
[14] R. Sarroukh, E. Cerf, S. Derclaye, Y.F. Dufrene, E. Goormaghtigh, J.M. Ruysschaert, Transformation of amyloid β(1–40) oligomers into fibrils is characterized by a major change in secondary structure, Cell. Mol. Life Sci. 68 (8) (2011) 1429–1438.
[15] Krimm, S. and J. Bandekar, Vibrational spectroscopy and conformation of peptides, polypeptides, and proteins, in *Adv. Protein Chem.* 1986, Elsevier. p. 181-364.
[16] C. Xue, T.Y. Lin, D. Chang, Z. Guo, Thioflavin T as an amyloid dye: fibril quantification, optimal concentration and effect on aggregation, R. Soc. Open Sci. 4 (1) (2017), 160696.
[17] J. Ryu, K. Girigoswami, C. Ha, S.H. Ku, C.B. Park, Influence of multiple metal ions on β-amyloid aggregation and dissociation on a solid surface, Biochemistry 47 (19) (2008) 5328–5335.
[18] M.J.A. Klug Genevieve, D. Losic, S.S. Subasinghe, M.I. Aguilar, L.L. Martin, D.H. Small, β-Amyloid protein oligomers induced by metal ions and acid pH are distinct from those generated by slow spontaneous ageing at neutral pH, Eur. J. Biochem. 270 (21) (2003) 4282–4293.
[19] V. Foderà, M. Groenning, V. Vetri, F. Librizzi, S. Spagnolo, C. Cornett, et al., Thioflavin T hydroxylation at basic pH and its effect on amyloid fibril detection, J. Phys. Chem. B 112 (47) (2008) 15174–15181.
[20] A. Korasick David, J. Tanner John, Determination of protein oligomeric structure from small-angle x-ray scattering, Protein Sci. 27 (4) (2018) 814–824.
[21] O.S. Makin, E. Atkins, P. Sikorski, J. Johansson, L.C. Serpell, Molecular basis for amyloid fibril formation and stability, Proc. Natl. Acad. Sci. U. S. A. 102 (2) (2005) 315.
[22] R. Nelson, M.R. Sawaya, M. Balbirnie, A. Madsen, C. Riekel, R. Grothe, D. Eisenberg, Structure of the cross-β spine of amyloid-like fibrils, Nature 435 (2005) 773.
[23] F.R. Kersey, W.C. Yount, S.L. Craig, Single-molecule force spectroscopy of bimolecular reactions: system homology in the mechanical activation of ligand substitution reactions, J. Am. Chem. Soc. 128 (12) (2006) 3886–3887.
[24] Z. Lv, R. Roychaudhuri, M.M. Condron, D.B. Teplow, Y.L. Lyubchenko, Mechanism of amyloid β-protein dimerization determined using single – molecule AFM force spectroscopy, Sci. Rep. 3 (2013) 2880.
[25] M. Murat, G.S. Grest, Molecular dynamics simulations of the force between a polymer brush and an AFM tip, Macromolecules 29 (25) (1996) 8282–8284.
[26] J. Yu, S. Malkova, Y.L. Lyubchenko, α-Synuclein misfolding: single molecule AFM force spectroscopy study, J. Mol. Biol. 384 (4) (2008) 992–1001.
[27] B. Ma, R. Nussinov, Simulations as analytical tools to understand protein aggregation and predict amyloid conformation, Curr. Opin. Chem. Biol. 10 (5) (2006) 445–452.
[28] A. Baumketner, S.L. Bernstein, T. Wyttenbach, G. Bitan, D.B. Teplow, M.T. Bowers, et al., Amyloid β-protein monomer structure: a computational and experimental study, Protein Sci. 15 (3) (2006) 420–428.
[29] X. Daura, K. Gademann, B. Jaun, D. Seebach, W.F. Gunsteren, A.E. Mark, Peptide folding: when simulation meets experiment, Angew. Chem. Int. Ed. 38 (1-2) (1999) 236–240.
[30] T. Ando, High-speed atomic force microscopy coming of age, Nanotechnology 23 (6) (2012), 062001.
[31] A.J. Katan, C. Dekker, High-speed AFM reveals the dynamics of single biomolecules at the nanometer scale, Cell 147 (5) (2011) 979–982.
[32] L. Picco, L. Bozec, A. Ulcinas, D.J. Engledew, M. Antognozzi, M.A. Horton, et al., Breaking the speed limit with atomic force microscopy, Nanotechnology 18 (4) (2006), 044030.
[33] Y. Lyubchenko, L. Shlyakhtenko, Atomic force microscopy imaging and probing of amyloid nanoaggregates, Handbook of Clinical Nanomedicine (2016) 589–616.
[34] T. Watanabe-Nakayama, K. Ono, M. Itami, R. Takahashi, D.B. Teplow, M. Yamada, High-speed atomic force microscopy reveals structural dynamics of amyloid β1–42 aggregates, Proc. Natl. Acad. Sci. 113 (21) (2016) 5835–5840.
[35] S. Banerjee, Z. Sun, E.Y. Hayden, D.B. Teplow, Y.L. Lyubchenko, Nanoscale dynamics of amyloid β-42 oligomers as revealed by high-speed atomic force microscopy, ACS Nano 11 (12) (2017) 12202–12209.
[36] K. Janek, S. Rothemund, K. Gast, M. Beyermann, J. Zipper, H. Fabian, et al., Study of the conformational transition of Aβ (1–42) using d-amino acid replacement analogues, Biochemistry 40 (18) (2001) 5457–5463.
[37] Y. Fezoui, D.B. Teplow, Kinetic studies of amyloid β-protein fibril assembly differential effects of α-helix stabilization, J. Biol. Chem. 277 (40) (2002) 36948–36954.
[38] T. Kowalewski, D.M. Holtzman, In situ atomic force microscopy study of Alzheimer's β-amyloid peptide on different substrates: new insights into mechanism of β-sheet formation, Proc. Natl. Acad. Sci. 96 (7) (1999) 3688–3693.
[39] J.D. Harper, C.M. Lieber, P.T. Lansbury Jr., Atomic force microscopic imaging of seeded fibril formation and fibril branching by the Alzheimer's disease amyloid-β protein, Chem. Biol. 4 (12) (1997) 951–959.
[40] H. Blackley, G.H.W. Sanders, M.C. Davies, C.J. Roberts, S.J.B. Tendler, M.J. Wilkinson, In-situ atomic force microscopy study of β-amyloid fibrillization, J. Mol. Biol. 298 (5) (2000) 833–840.
[41] W.B. Stine, L. Jungbauer, C. Yu, M.J. Ladu, Preparing synthetic Aβ in different aggregation states, Methods in molecular biology (Clifton, N.J.) 670 (2011) 13–32.

[42] N.J. Economou, M.J. Giammona, T.D. Do, X. Zheng, D.B. Teplow, S.K. Buratto, et al., Amyloid β-protein assembly and Alzheimer's disease: dodecamers of Aβ42, but not of Aβ40, seed fibril formation, J. Am. Chem. Soc. 138 (6) (2016) 1772–1775.
[43] Y. Prabhu, P.V. Burgos, C. Schindler, G.G. Farias, J.G. Magadan, J.S. Bonifacino, et al., Adaptor protein 2-mediated endocytosis of the β-secretase BACE1 is dispensable for amyloid precursor protein processing, Mol. Biol. Cell 23 (12) (2012) 2339–2351.
[44] N.G. Sgourakis, Y. Yan, S.A. McCallum, C. Wang, A.E. Garcia, The Alzheimer's peptides Aβ40 and 42 adopt distinct conformations in water: a combined MD/NMR study, J. Mol. Biol. 368 (5) (2007) 1448–1457.
[45] F. Massi, J.W Peng, J.E. Straub, Simulation study of the structure and dynamics of the Alzheimer's amyloid peptide congener in solution, Biophys. J. 80 (1) (2001) 31–44.
[46] P. Cizas, R. Budvytyte, R. Morkuniene, R. Moldovan, M. Broccio, M. Losche, et al., Size-dependent neurotoxicity of β-amyloid oligomers, Arch. Biochem. Biophys. 496 (2) (2010) 84–92.
[47] P.M. Gorman, C.M. Yip, P.E. Fraser, A. Chakrabartty, Alternate aggregation pathways of the Alzheimer β-amyloid peptide: Aβ association kinetics at endosomal pH, J. Mol. Biol. 325 (4) (2003) 743–757.
[48] A.E. Roher, M.O. Chaney, Y.M. Kuo, S.D. Webster, W.B. Sine, L. J. Haverkamp, et al., Morphology and toxicity of Aβ-(1–42) dimer derived from neuritic and vascular amyloid deposits of Alzheimer's disease, J. Biol. Chem. 271 (34) (1996) 20631–20635.
[49] K. Ono, M.M. Condron, D.B. Teplow, Structure–neurotoxicity relationships of amyloid β-protein oligomers, Proc. Natl. Acad. Sci. 106 (35) (2009) 14745–14750.
[50] D.J. Selkoe, Soluble oligomers of the amyloid β-protein impair synaptic plasticity and behavior, Behav. Brain Res. 192 (1) (2008) 106–113.
[51] M.E. Larson, S.E. Lesné, Soluble Aβ oligomer production and toxicity, J. Neurochem. 120 (s1) (2012) 125–139.
[52] S. Barghorn, V. Nimmrich, A. Striebinger, C. Krantz, P. Keller, B. Janson, et al., Globular amyloid β-peptide1–42 oligomer—a homogenous and stable neuropathological protein in Alzheimer's disease, J. Neurochem. 95 (3) (2005) 834–847.
[53] S.L. Bernstein, N.F. Dupuis, N.D. Lazo, T. Wyttenbach, M.M. Condron, G. Bitan, et al., Amyloid-β protein oligomerization and the importance of tetramers and dodecamers in the aetiology of Alzheimer's disease, Nat. Chem. 1 (4) (2009) 326–331.
[54] L. Tran, N. Basdevant, C. Prevost, T. Ha-Duong, Structure of ring-shaped Aβ 42 oligomers determined by conformational selection, Sci. Rep. 6 (2016) 21429.
[55] F. Meng, M.M.J. Bellaiche, JY. Kim, G.H. Zerze, R.B. Best, H. S. Chung, Highly disordered amyloid-β monomer probed by single-molecule FRET and MD simulation, Biophys. J. 114 (4) (2018) 870–884.
[56] N.-V. Buchete, R. Tycko, G. Hummer, Molecular dynamics simulations of Alzheimer's β-amyloid protofilaments, J. Mol. Biol. 353 (4) (2005) 804–821.
[57] B. Schuler, E.A. Lipman, W.A. Eaton, Probing the free-energy surface for protein folding with single-molecule fluorescence spectroscopy, Nature 419 (2002) 743.
[58] K.C. Neuman, A. Nagy, Single-molecule force spectroscopy: optical tweezers, magnetic tweezers and atomic force microscopy, Nat. Methods 5 (6) (2008) 491.
[59] S.A. Gittens, P.I. Kitov, J.R. Matyas, R. Lobenberg, H. Uludag, Impact of tether length on bone mineral affinity of protein–bisphosphonate conjugates, Pharm. Res. 21 (4) (2004) 608–616.
[60] J. Zlatanova, S.M. Lindsay, S.H. Leuba, Single molecule force spectroscopy in biology using the atomic force microscope, Prog. Biophys. Mol. Biol. 74 (1-2) (2000) 37–61.
[61] B.-H. Kim, N.Y. Palermo, S. Lovas, T. Zaikova, J.F.W. Keana, Y.L. Lyubchenko, Single-molecule atomic force microscopy force spectroscopy study of Aβ-40 interactions, Biochemistry 50 (23) (2011) 5154–5162.
[62] K. Zou, D. Kim, A. Kakio, K. Byun, JS. Gong, J. Kim, et al., Amyloid β-protein (Aβ) 1–40 protects neurons from damage induced by Aβ1–42 in culture and in rat brain, J. Neurochem. 87 (3) (2003) 609–619.
[63] F. Hane, S. Attwood, Z. Leonenko, Comparison of three competing dynamic force spectroscopy models to study binding forces of amyloid-β (1–42), Soft Matter 10 (12) (2014) 1924–1930.
[64] F.T. Hane, R. Hayes, B.Y. Lee, Z. Leonenko, Effect of copper and zinc on the single molecule self-affinity of Alzheimer's amyloid-β peptides, PLoS One 11 (1) (2016), e0147488.
[65] J.A. Schauerte, P.T. Wong, K.C. Wisser, H. Ding, D.G. Steel, A. Gafni, Simultaneous single-molecule fluorescence and conductivity studies reveal distinct classes of Aβ species on lipid bilayers, Biochemistry 49 (14) (2010) 3031–3039.
[66] X. Zhang, C. Liu, Z. Wang, Force spectroscopy of polymers: Studying on intramolecular and intermolecular interactions in single molecular level, Polymer 49 (16) (2008) 3353–3361.
[67] P. Hortschansky, V. Schroeckh, T. Christopeit, G. Zandomeneghi, M. Fandrich,, The aggregation kinetics of Alzheimer's β-amyloid peptide is controlled by stochastic nucleation, Protein Sci. 14 (7) (2005) 1753–1759.
[68] S. Nag, J. Chen, J. Irudayaraj, S. Maiti, Measurement of the attachment and assembly of small amyloid-β oligomers on live cell membranes at physiological concentrations using single-molecule tools, Biophys. J. 99 (6) (2010) 1969–1975.
[69] A. Orte, N.R. Birkett, R.W. Clarke, G.L. Devlin, C.M. Dobson, D. Klenerman, Direct characterization of amyloidogenic oligomers by single-molecule fluorescence, Proc. Natl. Acad. Sci. 105 (38) (2008) 14424–14429.
[70] J. Gsponer, U. Haberthür, A. Caflisch, The role of side-chain interactions in the early steps of aggregation: molecular dynamics simulations of an amyloid-forming peptide from the yeast prion Sup35, Proc. Natl. Acad. Sci. 100 (9) (2003) 5154–5159.
[71] M. Fändrich, V. Forge, K. Buder, M. Kittler, C.M. Dobson, S. Diekmann, Myoglobin forms amyloid fibrils by association of unfolded polypeptide segments, Proc. Natl. Acad. Sci. 100 (26) (2003) 15463–15468.
[72] M. Bucciantini, E. Giannoni, F. Chiti, F. Baroni, L. Formigli, J. Zurdo, et al., Inherent toxicity of aggregates implies a common mechanism for protein misfolding diseases, nature 416 (6880) (2002) 507.
[73] M. Reches, E. Gazit, Self-assembly of peptide nanotubes and amyloid-like structures by charged-termini-capped diphenylalanine peptide analogues, Israel Journal of Chemistry 45 (3) (2010) 363–371.
[74] T. Ando, T. Uchihashi, N. Kodera, High-speed AFM and applications to biomolecular systems, Annu. Rev. Biophys. 42 (1) (2013) 393–414.
[75] T. Uchihashi, N. Kodera, T. Ando, Guide to video recording of structure dynamics and dynamic processes of proteins by high-speed atomic force microscopy, Nat. Protoc. 7 (6) (2012) 1193.